Chemistry & Biology
Article

Structural and Mechanistic Analysis of Protein Interactions in Module 3 of the 6-Deoxyerythronolide B Synthase

Yinyan Tang,[1] Alice Y. Chen,[1] Chu-Young Kim,[1,3] David E. Cane,[2] and Chaitan Khosla[1,*]
[1]Departments of Chemistry and Chemical Engineering, Keck Building, Stanford University, Stanford, CA 94305, USA
[2]Department of Chemistry, Brown University, Providence, RI 02912, USA
[3]Present address: Department of Biological Sciences, National University of Singapore, 14 Science Drive 4, Singapore 117543, Singapore.
*Correspondence: khosla@stanford.edu
DOI 10.1016/j.chembiol.2007.07.012

SUMMARY

We report the 2.6 Å X-ray crystal structure of a 190 kDa homodimeric fragment from module 3 of the 6-deoxyerthronolide B synthase covalently bound to the inhibitor cerulenin. The structure shows two well-organized interdomain linker regions in addition to the full-length ketosynthase (KS) and acyltransferase (AT) domains. Analysis of the substrate-binding site of the KS domain suggests that a loop region at the homodimer interface influences KS substrate specificity. We also describe a model for the interaction of the catalytic domains with the acyl carrier protein (ACP) domain. The ACP is proposed to dock within a deep cleft between the KS and AT domains, with interactions that span both the KS homodimer and AT domain. In conjunction with other recent data, our results provide atomic resolution pictures of several catalytically relevant protein interactions in this remarkable family of modular megasynthases.

INTRODUCTION

Polyketide synthases (PKSs) comprise a large family of enzymes that catalyze the biosynthesis of structurally diverse and pharmacologically important natural products [1]. They assemble polyketide chains through repeated condensations between methylmalonyl or malonyl thioester building blocks and the growing polyketide acyl thioesters. Analogous to vertebrate fatty acid synthases, modular PKSs are large multienzyme assemblies that catalyze polyketide biosynthesis by an assembly line of active sites [2, 3]. In a typical PKS module, there are minimally three domains: a catalytic ketosynthase (KS) and acyltransferase (AT) domain, and an acyl carrier protein (ACP). The AT domain transfers an extender unit from the corresponding malonyl- or methylmalonyl-CoA substrate to the phosphopantetheine arm of the ACP. Upon receiving the growing polyketide chain from the appropriate upstream module, the KS domain catalyzes decarboxylative condensation between the resultant acyl-KS intermediate and the respective malonyl- or methylmalonyl extender unit to form a β-ketoacyl-ACP. The core catalytic domains of a PKS module are flanked by catalytically inactive 20–300 amino acid linker regions whose structure and function are only beginning to be understood [4–6].

6-Deoxyerthronolide B synthase (DEBS), which produces the macrocyclic core of the antibiotic erythromycin, is comprised of three homodimeric polypeptides subunits, each of which consists of more than 3000 amino acids (Figure 1). Each DEBS polypeptide is made up of two polyketide chain-elongation modules, with each module including all of the required catalytic domains responsible for one round of polyketide chain extension and β-keto group modification. As the prototypical modular PKS, DEBS has been intensively investigated over the past two decades [7]. The modular nature of DEBS, together with the medicinal significance of its product, has also made it an attractive target for the production of novel polyketides by combinatorial biosynthesis [8, 9]. While some notable success in engineering DEBS to produce novel macrolides has been achieved, the majority of engineered PKSs have suboptimal activity, arising at least in part from a lack of knowledge regarding precise domain boundaries [5, 10, 11]. Further progress in the engineering of the biosynthesis of novel polyketides requires detailed insights into the structure of DEBS and related modular PKSs.

We recently reported the 2.7 Å X-ray crystal structure of a 194 kDa homodimeric [KS][AT] fragment of DEBS module 5 [12]. In addition to the two pairs of catalytic KS and AT domains and the N-terminal docking domain, the structure also revealed two interdomain linker regions with well-defined three-dimensional structures that each show extensive interactions with the core catalytic domains. Although the overall primary sequences of these linker regions are less conserved compared to those of the corresponding catalytic domains, the amino acid residues responsible for specific domain-linker interactions are highly conserved in all six DEBS modules.

Here, we present the 2.6 Å structure of a homologous [KS][AT] fragment from DEBS module 3. In addition to

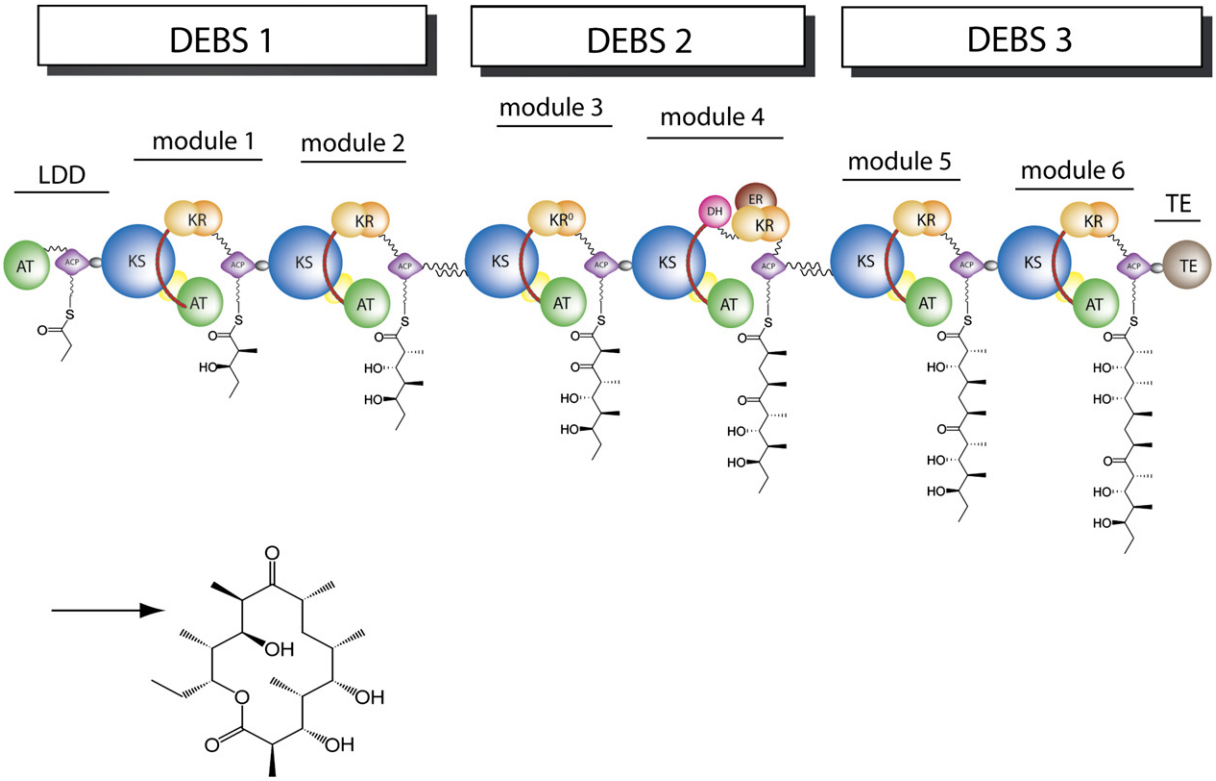

Figure 1. Modular Organization of 6-Deoxyerythronolide B Synthase Illustrating the Deduced Topology

6-Deoxyerythronolide B synthase (DEBS) contains three large homodimeric polypetides, each of which consists of two modules. Each module is minimally composed of a core set of ketosynthase (KS), acyltranferase (AT), and acyl carrier protein (ACP) domains. Additional ketoreductase (KR), dehydratase (DH), and enoylreductase (ER) domains are responsible for processing of the β-ketoacyl-SACP intermediates, while a specialized thioesterase (TE) domain releases the mature heptaketide chain with cyclization to generate the 6-deoxyerythonolide B product.

reconfirming the major architectural features of previously reported PKS modules and their constituent domains, the structure, which includes a covalently bound molecule of the inhibitor cerulenin, provides a clearer definition of the KS active site. A detailed comparison between the active sites of DEBS KS3 and KS5 reveals a set of residues that are thought to control specificity for their respective triketide and pentaketide substrates. Lastly, guided by the recently solved NMR structure of the ACP domain of DEBS module 2, we have proposed a plausible KS-ACP docking model that predicts both electrostatic and hydrophobic interactions at the critical domain-domain interface.

RESULTS AND DISCUSSION

Catalytic Activity of the Crystallized Fragment of DEBS Module 3

Motivated by our earlier success with DEBS module 5, we initially prepared and attempted to crystallize the full-length [KS3][AT3] didomain protein with its intact N-terminal docking domain as well as the KS-to-AT and post-AT linkers. Unfortunately, no diffracting crystals could be obtained from this recombinant protein. Guided by encouraging preliminary data for a 190 kDa proteolytic fragment of this protein from which the N-terminal docking domain had been cleaved [13], we expressed the recombinant protein corresponding to this trypsin fragment and purified it to homogeneity. The KS acylation activity as well as the chain-elongation properties of the purified protein were assayed, so as to assess the catalytic consequences of removing the N-terminal docking domain. Both activities were preserved in this truncated form of module 3, albeit at 30% of the activity of the intact [KS][AT] didomain (data not shown). The recombinant truncated protein was therefore used for initial crystallization screens, which yielded needle crystals. Having established preliminary crystallization conditions, the truncated protein was then incubated with cerulenin, a known active-site-directed irreversible inhibitor of the KS domains of numerous PKSs and fatty acid synthases, and the protein-cerulenin adduct was purified prior to protein crystallization. In a separate set of experiments, the recombinant protein was also incubated with (2*S*,3*R*)-2-methyl-3-hydroxypentanoyl-*N*-acetylcysteamine thioester, and the resulting acylated protein was purified for crystallization. Only the protein incubated with cerulenin gave diffractable crystals.

Overall Structure

The cerulenin-inhibited form of the 190 kDa fragment of DEBS module 3 was crystallized at room temperature by

the hanging-drop method. The protein crystallized in space group $P2_1$ with one homodimer per asymmetric unit. The crystal structure was determined by molecular replacement with the recently determined structure of the [KS5][AT5] didomain from DEBS module 5 (PDB ID: 2HG4) as the search model. The structure was refined to 2.6 Å resolution, with R and R_{free} values of 21.8% and 26.8%, respectively. The final protein model after refinement contained 869 out of the 896 residues of the subunit; no electron density was observed for 2 N-terminal residues, 14 C-terminal residues, and 11 residues from 2 internal disordered regions. In each monomer, the cerulenin molecule was only partially defined by the electron density, suggesting that the octadienyl moiety of the inhibitor that is distal to the point of attachment to the active site cysteine is relatively flexible and therefore disordered in the crystal. Data, refinement, and model statistics are summarized in Table 1.

Notwithstanding the absence of the N-terminal docking domain, the overall organization of the truncated [KS3][AT3] didomain protein of DEBS module 3 is very similar to that of the [KS5][AT5] protein from DEBS module 5 (Figure 2). The homodimeric [KS3][AT3] protein has two catalytic domains, KS3 and AT3, and two linker regions, the KS-to-AT linker and the post-AT linker. The dimer interface is located solely between the two KS domains. Similar to other condensing enzymes from fatty acid synthases and PKSs, each KS3 domain adopts the five-layered αβαβα fold, first observed in thiolase [12, 14–18]. The dimer interface is primarily comprised of two antiparallel β strands, one from each subunit, that are held together by backbone hydrogen bonds, thereby creating a ten-stranded β sheet. The salt bridges previously observed at the KS5 dimer interface are not found in the corresponding KS3 dimer interface. Superposition of the C_α atoms of the KS3 and KS5 domains gives an rmsd of 0.85 Å for 386 C_α atoms. A noticeable difference between the KS3 and KS5 domain is that KS3 has a longer loop corresponding to residues 71–91. Sequence alignment among the six DEBS KS domains shows that only KS5 is 12 residues shorter than other KS domains in this region, indicating that the remaining KS domains will have a loop of similar length to that of the KS3 domain.

The architecture of the AT3 domain is similar to that of the *Escherichia coli* and the *Streptomyces coelicolor* malonyl-CoA:ACP transferases, as well as the DEBS AT5 domain [12, 19, 20]. The AT3 domain has an α,β-hydrolase core and an appended smaller subdomain with a ferredoxin-like structure. The structures of the DEBS AT3 and AT5 domains can be superimposed with an rmsd of 1.1 Å for 292 C_α atoms.

The ~100 residue-long KS-to-AT linker of the [KS3][AT3] protein is also structurally homologous to its [KS5][AT5] counterpart, with only a 1.54 Å rmsd between the backbone atoms of the two KS-to-AT linkers, in spite of the fact that the overall sequence similarity (47%) between the two interdomain linkers is less than that between the corresponding pairs of KS and AT catalytic domains (~60%). The KS3-to-AT3 linker contains a three-stranded parallel β sheet, flanked by three α helices on one side and two α helices on the other. Similar to the KS5-to-AT5 linker, the three α helices on one side are part of the KS3-to-AT3 linker itself, while the two α helices on the other side are contributed by the AT3 domain and the post-AT linker, respectively. Finally, the post-AT linker wraps around both the AT3 domain and the KS-to-AT linker so as to engage in extensive contacts with the KS3 domain. The previously observed, highly conserved hydrophobic interactions between the two linkers and the two catalytic domains of [KS5][AT5] are also observed in the [KS3][AT3] protein. Specifically, the conserved residues Phe102, Phe106, Phe107, Val109, Ala114, Leu125, Trp129, Pro139, Met189, His516, Tyr898, and Phe900 comprise the hydrophobic core between the two linkers and the KS3 domain, while Pro473, Val475, Leu507,

Table 1. Data Collection and Structure Refinement Statistics

Data Collection Statistics	
Wavelength (Å)	0.979
Resolution (Å)	2.60
Reflection (observed/unique)	22,8717/62,083
Completeness (%)	99.8 (100)
Redundancy	3.7 (3.7)
I/σ(I)	16.0 (3.1)
R_{merge} [a]	0.135 (0.688)
Refinement Statistics	
Space group	$P2_1$
Unit cell parameters	a = 75.203 Å, b = 139.005 Å, c = 102.342 Å, γ = 106.14°
Monomers per A.U.	2
Protein atoms	12,944
Water molecules	194
R_{free} [b] (%)	26.8
R_{crys} [c] (%)	21.8
Rms deviation	
Bonds (Å)	0.017
Angles (°)	1.94
Ramachandran plot (%)	
Most favored	84.2
Additionally favored	13.4
Generously allowed	1.4
Disallowed	1.0

[a] $R_{merge} = \Sigma|I_o - \langle I\rangle|/\Sigma\langle I\rangle$ summed over all observations and reflections.
[b] $R_{free} = R_{cryst}$ calculated for 5% of reflections omitted from the refinement.
[c] $R_{cryst} = \Sigma|F_o - F_c|/\Sigma|F_o|$.

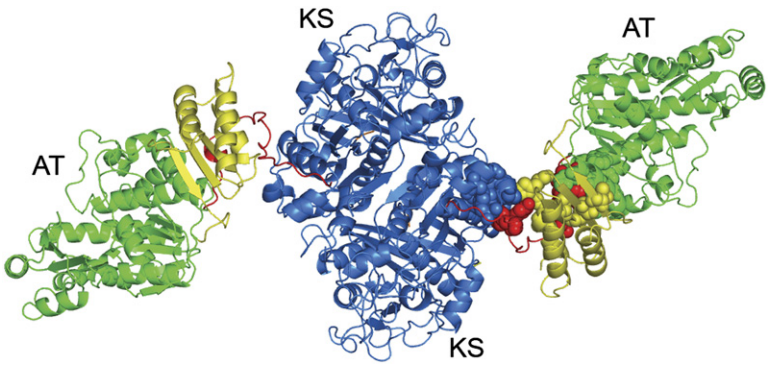

Figure 2. X-Ray Crystal Structure of the [KS3][AT3] Didomain of DEBS Module 3
The protein forms a homodimer. The KS3 domain, the KS3-to-AT3 linker, the AT3 domain, and the post-AT linker are shown in blue, yellow, green, and red, respectively. The conserved hydrophobic cores at the domain-linker interfaces of one monomer are shown as colored spheres.

Ala510, Ala521, Val548, Trp637, Tyr640, Phe867, Leu868, Met871, Ala872, His875, Ile881, Trp883, and Leu887 form the hydrophobic core between the two linkers and the AT3 domain (Figure 2).

In the [KS5][AT5] protein, the N-terminal docking domains from the two monomers form an extended coiled-coil structure, contributing to the homodimer interface [12, 21]. The corresponding N-terminal residues involved in the coiled-coil interface are well conserved in the native DEBS module 3. It is therefore reasonable to expect that the N-terminal docking domain in the full-length [KS3][AT3] protein also forms a similar coiled-coil structure. In the truncated [KS3][AT3] protein, the 4 residues, E27-L28-E29-S30, at the N terminus belong to the original N-terminal docking domain of DEBS module 3. While no electron density was detected for the first two of these amino acids, the next 2 residues are visible in the [KS3][AT3] structure. As shown in Figure 3A, Glu29-Ser30-Asp31 at the N terminus of KS3 do not overlap with the corresponding region of the [KS5][AT5] protein, in which the intact coiled-coil N-terminal docking domain is present (Figure 3A). Beyond this local difference, the excision of the N-terminal docking domain from KS3 has little apparent effect on the overall KS3 dimer geometry.

Although the individual KS domain, KS-to-AT linker, and AT domain structures are well conserved between the [KS3][AT3] and [KS5][AT5] proteins, a significantly higher net rmsd of 4.2 Å is observed when the entire structures of both proteins are superimposed (Figure 3B). A close inspection of the superimposed structures shows that this divergence stems from a rotation of ~26° of the AT3 domain. As a result, the cleft between each AT3 domain

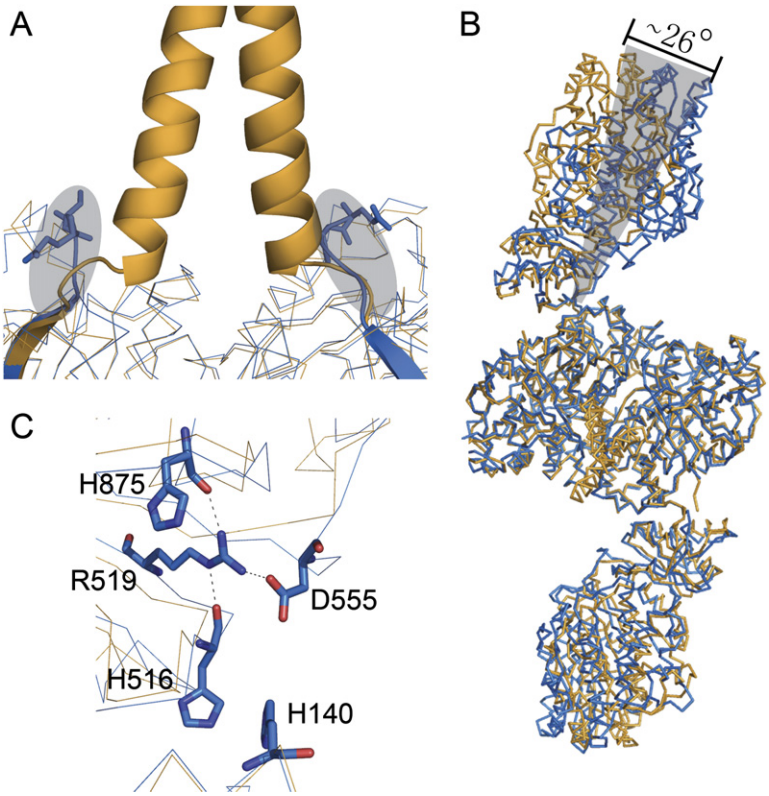

Figure 3. Comparison of the Structures of the [KS3][AT3] Didomain and the [KS5][AT5] Didomain
(A) The coiled-coil N-terminal docking domain of the [KS5][AT5] didomain (orange) is shown. The residues E29–S30 at the N terminus of [KS3][AT3] (blue) are shown in sticks. The difference in the region of the N-terminal docking domains is depicted in the shadowed area.
(B) Superposition of the complete backbones of the two didomains. The AT3 domain is rotated ~26° relative to the orientation of the AT5 domain.
(C) Domain-domain interactions in the [KS3][AT3] didomain. Asp555 forms a salt bridge with Arg519; the latter residue is also hydrogen bonded to His516 and H140.

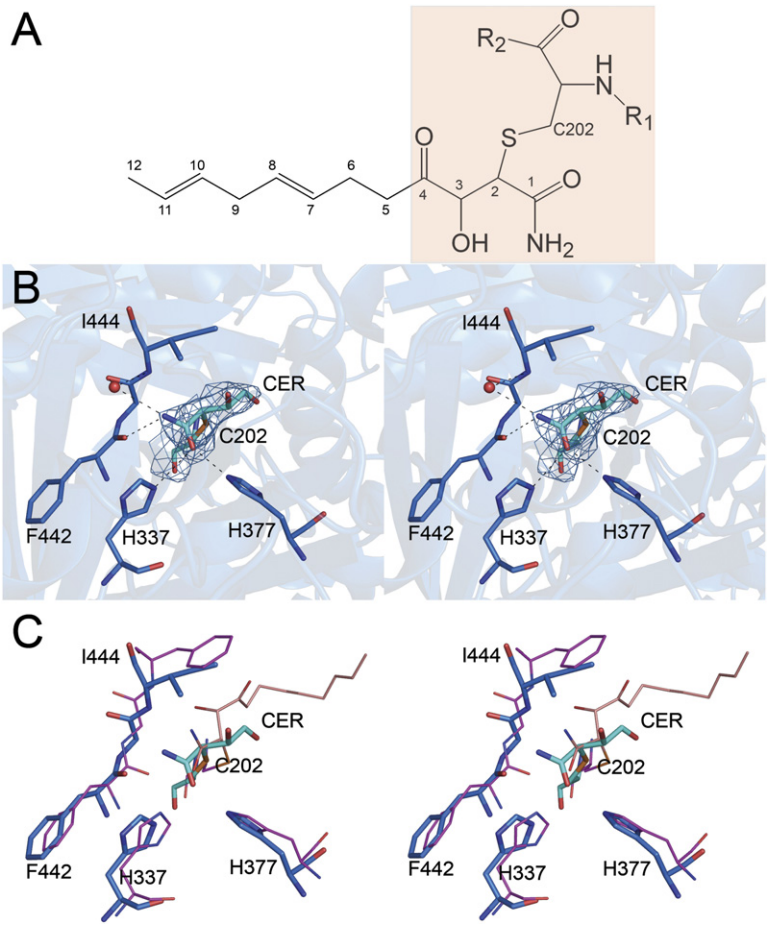

Figure 4. The Cerulenin-Binding Site in the [KS3][AT3] Didomain

(A) The cerulenin molecule is covalently bound to the enzyme; only the shaded portion is visible in the electron density map.

(B) Stereoview of the final $2F_o - F_c$ map at the cerulenin (cyan)-binding site contoured at 1.0 Å.

(C) Stereoview of the structure of the FabF-cerulenin complex (magenta) superimposed on the structure of the [KS3][AT3]-cerulenin didomain (blue).

and the KS3 dimer is smaller compared to its [KS5][AT5] counterpart. The origin of this relatively "closed" conformation of the [KS3][AT3] protein is unclear. It could be a crystallization artifact due to crystal packing; alternatively, the cleavage of the N-terminal docking domain may contribute to this "closed" conformation, since this truncated [KS3][AT3] only exhibits 30% of the activity of the full-length protein. Nonetheless, this relatively "closed" conformation appears to be stabilized by a series of specific interactions, including hydrogen bonding and charge-charge interactions, that are absent in [KS5][AT5] (Figure 3C). For example, Asp555 forms a hydrogen bond with the side chain of Arg519, whose orientation is fixed by hydrogen bonding to the backbone carbonyl oxygens of both His516 and His875. In addition, Asp555 is also engaged in charge-charge interactions with side chains of both His140 and His516. Aside from Arg519 and His875, none of the residues involved in the above-described interactions are conserved among the six DEBS KS domains.

The Cerulenin-Binding Site in KS3

Analogous to other fatty acid synthase and polyketide synthase condensing enzymes, the active site of the KS3 domain is buried, and therefore only accessible by the 18 Å phosphopantetheine arm of an ACP [12]. The active site Cys202 residue of KS3 resides in a nucleophilic elbow in a tight turn between a β strand and an α helix. His337 and His377, which form part of the catalytic triad, are located adjacent to Cys202. Besides providing an oxyanion hole to promote nucleophilic attack on the carbonyl of the acylthioester, these histidine residues have also been implicated in catalyzing decarboxylation of the co-substrate methylmalonyl-*S*-ACP [22, 23]. In the electron density map of the [KS3][AT3]-cerulenin complex, only the four-carbon hydrophilic head and attached groups of the cerulenin adduct are visible, albeit with a higher B factor than the rest of the protein (Figures 4A and 4B). The electron density corresponding to the hydrophobic octadienyl tail of the inhibitor is missing, presumably because of conformational disorder. A covalent bond is observed between C-2 of the cerulenin adduct and the active site Cys202. The carbonyl oxygen of the terminal carboxamide hydrogen bonds with the NE atoms of His337 and His377, while the carboxamide nitrogen is within hydrogen-bonding distance of the backbone carbonyl oxygen of Phe442 and a water molecule. No other contacts are observed between the cerulenin adduct and the protein.

To date, two crystal structures of KS-cerulenin complexes have been reported for β-ketoacyl-ACP:ACP

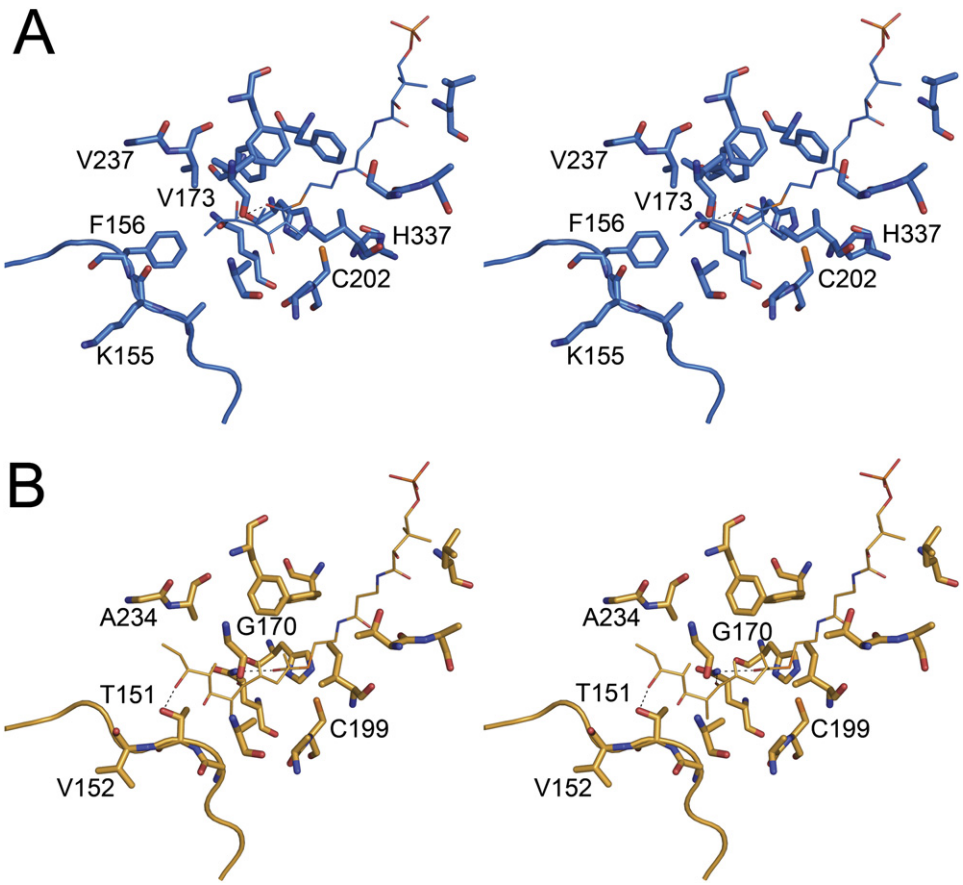

Figure 5. Substrate-Binding Models for the Active Sites of KS3 and KS5

(A) Model of the triketide-phosphopantetheine group in the KS3 active site showing proposed interactions with residues lining the substrate-binding pocket.

(B) Model of the pentaketide-phosphopantetheine group in the KS5 active site showing proposed interactions with residues lining the substrate-binding pocket.

synthases of type II fatty acid synthases, FabB-cerulenin and FabF-cerulenin [24, 25]. When the structure of cerulenin-bound [KS3][AT3] is superimposed on that of FabF-cerulenin, (Figure 4C), C-1 and C-2 of the covalently attached inhibitor occupy almost identical positions in the two proteins, while C-3 and C-4 are rotated more than 120° in the [KS3][AT3] complex relative to the FabF complex. This rotation may reflect the conformation of the flexible hydrophobic octadienyl tail of cerulenin in the [KS3][AT3] active site, since cerulenin has a lower binding affinity to KS domains from PKSs compared to those from fatty acid synthases [26].

Substrate Specificity of the KS Domain: Comparing DEBS KS3 to KS5

DEBS KS3 and KS5 share 60% sequence identity but have different substrate specificities. The natural substrate of KS3 is a triketide, whereas the natural substrate of KS5 is a pentaketide (Figure 1). While KS3 can be stoichiometrically acylated by the N-acetylcysteamine thioester derivative of the natural diketide product of DEBS module 1, KS5 is acylated more slowly by this same analog under the same conditions.

To better understand the structural basis for KS substrate specificity, we docked the natural triketide substrate of KS3, bound to a phosphopantetheinyl arm, into the substrate-binding pocket of KS3. This simulated complex was then superimposed onto the corresponding KS5-pentaketide complex that had been modeled earlier [12]. As shown in Figure 5, there are two major differences between the substrate-binding pockets of the KS3 and KS5 domains. First, a loop found at the dimer interface in both proteins (residues 153–158 in KS3 and 149–154 in KS5) has substantially different conformations in the otherwise very similar proteins. Compared to KS3, this loop is more extended in KS5. This difference in loop conformation results in the side chains of 2 KS3 residues (Lys155 and Phe156) being oriented in opposite directions compared to the corresponding KS5 residues, Thr151 and Val152. The orientation of Thr151 in KS5 is thought to be important for binding of its pentaketide substrate, based on a predicted hydrogen bond between the threonine

side chain hydroxyl and the C-9 hydroxyl of the substrate. The counterpart Lys155 residue in KS3 points away from the substrate-binding site. In addition, KS3 has more bulky residues in the active site than does KS5. For example, Phe156, Val173, and Val237 in KS3, which presumably interact with the untethered end of the polyketide chain, correspond to the smaller Val152, Gly170, and Ala234, respectively, in KS5. The resulting steric differences could influence the preferred substrate size that can be accommodated in the two different active sites.

It must be noted, however, that neither substrate-binding pocket is especially crowded and each may therefore readily undergo modest conformational adjustments upon substrate binding. Indeed, such conformational flexibility may be the origin of the observed relative substrate promiscuity of modular PKSs [27].

Interaction between the [KS][AT] Homodimer and an ACP Domain

During polyketide biosynthesis, the ACP domain interacts with several catalytic sites, in each case serving as a scaffold to which the malonyl- or methylmalonyl extender unit and the growing polyketide chain are alternately tethered. A number of recent studies have highlighted the critical importance of KS:ACP specificity, both during intermodular chain transfer as well as during the intramodular KS-catalyzed decarboxylative condensation reactions [28–30]. Understanding the structural basis for this protein:-protein specificity is of critical importance to the rational engineering of catalytically efficient PKSs.

In addition to knowledge of the [KS3][AT3] structure, computational prediction of the KS-ACP interface requires an accurate molecular model for the cognate ACP partner. Until recently, no structures were available for ACP domains derived from modular PKSs. Although the structures of more distantly related carrier proteins have been solved [31–38], their level of sequence identity with the DEBS ACP domains (<25%) is lower than the pairwise sequence identities between DEBS ACP domains (45%–55%). We have recently solved the solution NMR structure of a recombinant ACP domain derived from DEBS module 2 and used this structure to derive homology models for the six remaining DEBS ACP domains, including ACP3 [39]. We have now utilized the solution NMR structure of ACP2 (the cognate partner of KS3 during intermodular chain transfer) as well as the homology model of ACP3 (the cognate partner of KS3 during chain elongation) in computational docking studies in order to gain insight into the interface between the [KS3][AT3] protein and its partner ACP2 and ACP3 domains.

The 3D-Dock [40] and Patchdock servers [41, 42] were used for individual computational docking simulations between both the ACP2 and ACP3 domains and the [KS3][AT3] protein. The two programs yielded similar docking results for both ACPs. As shown in Figures 6A and 6B, the most favorable ACP docking site, predicted based on a combination of binding energy and shape complementary, is the deep cleft between the KS3 and AT3 domains. The orientations of ACP2 and ACP3 predicted by the docking models are not identical; both the N terminus and the C terminus of ACP3 are relatively closer to the AT3 domain compared to ACP2. Nonetheless, the two docking models share important common features. Notably, while the ACPs are docked in the cleft of [KS3][AT3] subunit A, the active site residue Ser is actually positioned so as to direct its pantetheinyl prosthetic group and attached substrate to the active site of the KS domain of the paired subunit B. The validity of the calculated docking models is supported by three observations. First, the Ser54 residues of both ACP2 and ACP3, to which the 18 Å phosphopantetheinyl arms are covalently attached, are predicted to be positioned near the entrance of the substrate-binding pocket of one KS3 monomer B, ~20 Å from the active site Cys202. Second, the docking model predicts that each ACP domain will interact with both subunits of the KS dimer. In a recently reported crystal structure of the yeast fatty acid synthase, the ACP was observed to preferentially bind to the KS domain, and to interact with both subunits of the KS dimer, but functional interaction was limited to one subunit of the KS dimer [43]. Although the overall architecture of the yeast fatty acid synthase is distinct from modular PKSs such as DEBS, it is likely that interaction between the core domain of yeast ACP and the yeast KS domain is similar to that in modular PKSs. Third, the crystal structure of the yeast FAS also revealed that helix II of the core domain of ACP is important for KS recognition [43]. In the ACP docking model, the KS2-ACP2 and KS2-ACP3 interfaces both include helix II of each ACP. For example, Arg61 of helix II of ACP3 is predicted to form a hydrogen bond with Asn303 of KS3, while Leu55 from helix II of ACP2 is involved in hydrophobic interactions with KS3.

One interesting question arises from the docking model: To which subunit of the homodimeric module does the docked ACP3 belong? Previous mutant complementation and crosslinking studies carried out in our lab have shown that the ACP from one subunit preferentially interacts with the KS domain from the opposite subunit [44]. In the ACP3 docking model, the C-terminal end of the post-AT linker from [KS3][AT3] subunit A is indeed 16 Å closer to the N terminus of the docked ACP3 domain than is the corresponding C terminus of the post-AT linker belonging to [KS3][AT3] subunit B. It is therefore tempting to conclude that the illustrated ACP3 should belong to subunit A of the homodimer (Figure 6B). This may be the case for those PKS modules that consist only of the three core KS, AT, and ACP domains, in which the location of the ACP is constrained only by the length of the AT-to-ACP linker. On the other hand, since the native DEBS module 3 also harbors an inactive KR domain (Figure 1), the position of the ACP domain is restrained not only by the KR-to-ACP linker, but also by the KR domain itself. Since, in the proposed structure model for the full DEBS module 3 [45], it is not yet possible to assign the individual KR domains to a given subunit, it is therefore premature to try to assign the docked ACP to a specific subunit of the homodimer pending the availability of an atomic resolution structure of the entire module.

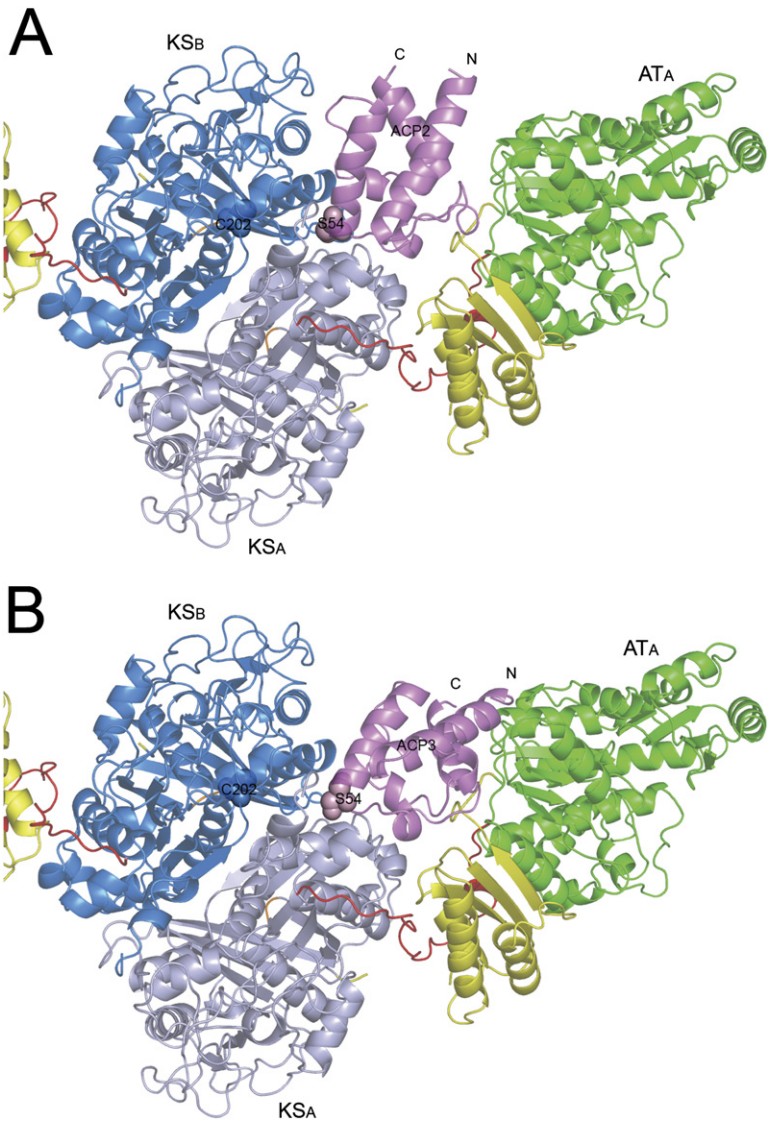

Figure 6. Calculated Docking Model for the Interaction between ACP Domains and the [KS3][AT3] Didomain

(A and B) The ACP domains are shown as violet ribbons. The active site residues of the ACP and KS domains are shown as spheres. The [KS3][AT3] domain is shown in the same orientation as in Figure 2. (A) Model of ACP2 docked in the KS-AT cleft of the [KS3][AT3] didomain. (B) Model of ACP3 docked in the KS-AT cleft of the [KS3][AT3] didomain.

An important feature of the ACP2 and ACP3 docking models is that both ACP domains are predicted to interact not only with both halves of the KS3 homodimer, but also with a considerable portion of the remainder of the [KS3][AT3] protein. In the discussion that follows, for brevity only the ACP3 docking model is analyzed in detail.

A total of 1628 $Å^2$ surface area is predicted to be buried upon ACP3 binding, while the surface area buried between the KS3 homodimer and ACP3 is only 983 $Å^2$. In fact, in a companion study carried out in our lab, we have shown that the efficiency of recognition of ACP3 by the KS3 domain is greatly enhanced by the presence of both the AT3 domain and the post-AT linker [46]. The interactions predicted to occur at the [KS3][AT3]-ACP3 interface are due to the contacts between ACP3 and the KS3 homodimer and the contacts between ACP3 and the rest of the [KS3][AT3] protein.

The interface between ACP3 and the KS3 homodimer involves both hydrophobic and hydrophilic interactions. For example, Phe78 of the ACP3 is predicted to bind in a hydrophobic KS3 core region (Figure 7). As illustrated by the multiple sequence alignment (Figure S1; see the Supplemental Data available with this article online), Phe78 of ACP3 is in fact strictly conserved in type I PKSs, but not in type II PKSs. The same is true for the deduced hydrophobic cores in the corresponding type I KS domains or type II proteins (sequences not shown). In the NMR solution structure of ACP2 and the homology model of ACP3, Phe78 is located on the protein surface, with its side chain pointing away from the protein. Interestingly, in the carrier protein domains (thiolation or T domains) of the enterobactin nonribosomal peptide synthetase, the residues that align with Phe78 of ACP3 have been shown to play key roles in mediating protein-protein interactions [47, 48]. In the latter system, mutation of Ala268 to Gln in the EntB-ArCP degraded interaction with EntF, leading to a 90-fold reduction in the rate of enterobactin production [47]. In a like manner, mutation of

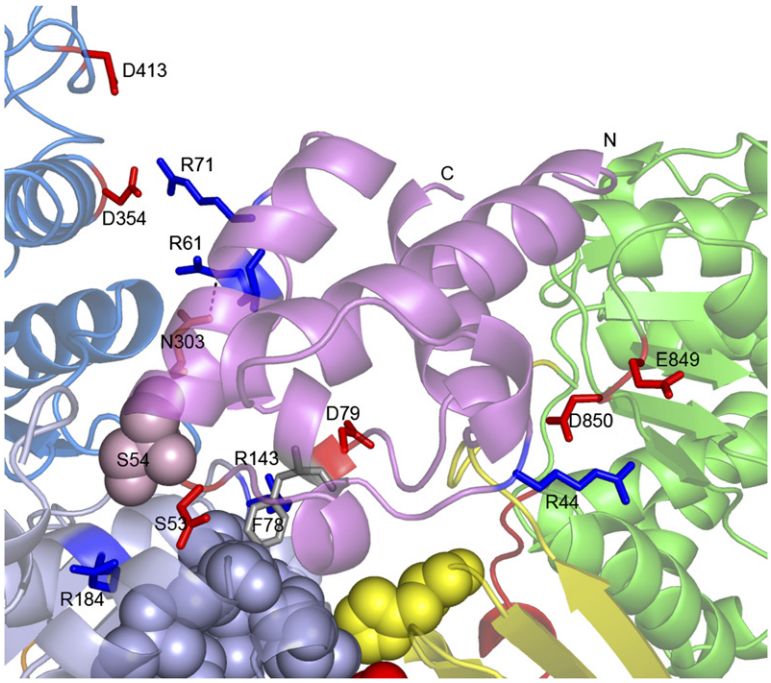

Figure 7. Close-Up View of the ACP3 Docking Model

The residues involved in ACP-KS and ACP-AT charge-charge interactions are shown as sticks, and the KS and KS-to-AT linker residues involved in hydrophobic interactions with ACP3 are shown as gray and yellow, respectively, spheres.

the corresponding residue in the EntF-T domain abolished transfer of the acetyl group from the T to the thioesterase (TE) domain, indicating the crucial role of this residue in T-TE interaction [48]. Together, those observations reinforce the idea that Phe78 of ACP3 may be important for protein-protein interactions in DEBS KS3.

To directly investigate the role of Phe78 of the ACP3 domain, this residue was mutated to a charged Asp residue in order to disrupt the proposed hydrophobic interactions with the conserved hydrophobic core of the [KS][AT] didomain. Circular dichroism (CD) analysis confirmed the structural integrity of the F78D mutant relative to the wild-type ACP3 (Figure S2). The steady-state kinetic parameters were determined for the F78D mutant by assaying the conversion of the diketide substrate, (2*S*,3*R*)-2-methyl-3-hydroxypentanoyl-*N*-acetylcysteamine thioester, to the corresponding triketide ketolactone catalyzed by [KS3][AT3] [30]. The [KS3][AT3] protein was first incubated with the diketide to effect acylation, and then [^{14}C]methylmalonyl-CoA and ACP3 (WT or F78D) were added to the mixture. After incubation for an appropriate amount of time, the reaction was quenched and the derived triketide ketolactone was quantified (Figure S3 and Table S1). Mutation of F78D resulted in a modest decrease in efficiency of triketide lactone formation, as reflected in a 2-fold decrease in k_{cat} as well as a 2-fold increase in K_M, resulting in a net 4-fold reduction in catalytic efficiency (k_{cat}/K_M) relative to the wild-type ACP3. These results suggest that Phe78 may contribute, but is not critical for, to the interaction between ACP3 and [KS3][AT3].

The hydrophilic interactions at the KS3-ACP3 interface involve several charged residues. In addition to the hydrogen bond between Arg61 of ACP3 and Asn303 of KS3, Asp53 and Asp79 of ACP3 are likely involved in charge-charge interactions with Arg184 and Arg143 of KS3, respectively; these 4 residues are strictly conserved in all DEBS modules. Additional charge-charge interactions are predicted between Arg71 of ACP3 and Asp354 and Asp413 of KS3. None of these residues are conserved among other DEBS modules, suggesting that this electrostatic interaction may contribute to the observed KS:ACP recognition specificity [30].

The interaction at the interface of ACP3 and AT3 in the ACP3 docking model involves Arg44 of ACP3 and Glu849 and Asp850 of AT3. None of these 3 residues are conserved in the remaining five DEBS modules, suggesting that these charge-charge interactions may also contribute to the KS3:ACP3 specificity [30]. Since it is has been shown that KS3 and KS6 have orthogonal specificities toward ACP3 and ACP6, we wanted to test whether mutations around Arg44 of ACP3 could change the KS:ACP recognition specificity. Arg44 and Arg45 of ACP3 were therefore mutated to Asp and Gln, respectively, corresponding to the homologous residues of ACP6. Two single mutants—R44D, R45Q—and one double mutant—R44D/R45Q—were constructed. The CD spectra of the mutants showed characteristics of an α-helical conformation, suggesting equivalent tertiary structures of the mutants and wild-type ACP3 (Figure S2). The polyketide chain-elongation assay was carried out by using [KS3][AT3] or [KS6][AT6] in combination with these three mutants. As shown in Figure S4, the two single mutants behaved similarly to the wild-type. Thus, no triketide ketolactone formation was observed when the two single ACP3 mutants were incubated with [KS6][AT6]. In contrast, the double mutant totally lost the ability of the wild-type to interact productively with

[KS3][AT3], but instead showed about 6% of the activity of wild-type ACP6. Taken together, the results of these experiments strongly suggest that specific hydrophilic interactions between ACP3 and KS3 involving Arg44 and Arg45 of ACP3 contribute to the observed KS3:ACP3 recognition specificity.

It should be stressed that functional interaction between ACP3 and the active site of the AT3 domain, from which the pantetheinyl group of ACP must acquire its methylmalonyl residue, cannot take place when ACP3 is bound as predicted into the cleft between the KS3 and AT3 domains. Similar to the [KS5][AT5] homodimer, the respective active site Cys and Ser residues of the KS3 and AT3 domains are separated by ~76 Å. A second, functionally distinct, ACP3-AT3 docking site must therefore be present on the face of the AT domain distal to the KS3-AT3 cleft. The latter interaction was not revealed, however, by the docking simulations.

SIGNIFICANCE

Modular PKSs are responsible for the biosynthesis of polyketide natural products with a variety of antibiotic, antiviral, immunosuppressant, cholesterol-lowering, and anticancer activities. The modular organization of these PKSs makes them attractive targets for engineering designed to allow for combinatorial biosynthesis of novel polyketide metabolites. Until now, however, the lack of detailed structural and mechanistic information for these megaenyzmes has greatly hampered progress in rational engineering of these modular polyketides, with primary sequence alignments being the only effective tool for predicting the boundaries of the constituent functional domains. The crystal structure of a 190 kDa homodimeric didomain fragment of DEBS module 3 with a covalently bound cerulenin at the KS3 active site provides important new, to our knowledge, insights into the structure and function of modular PKS proteins. The bound cerulenin also provides a more refined definition of both the KS3 and KS5 active sites. Detailed structural comparison between the structures of DEBS KS3 and KS5 highlight specific residues that may be important in determining both intrinsic substrate specificity and tolerance of the KS domains. Docking simulation with both the ACP2 NMR solution structure and an ACP3 homology model predicts that the ACP domain interacts with the KS domain by binding in the deep cleft between the KS and AT domains. Our results open the door to future efforts to engineer useful polyketide products with important medicinal activities.

EXPERIMENTAL PROCEDURES

Reagents and Chemicals

DL-[2-methyl-^{14}C]-methylmalonyl-CoA was purchased from American Radiolabeled Chemicals. (2*S*,3*R*)-2-methyl-3-hydroxypentanoyl-*N*-acetylcysteamine thioester was prepared by established methods [49–51]. All other chemicals were purchased from Sigma. Thin-layer chromatography (TLC) plates were a gift from J.T. Baker. SDS PAGE-gradient gels (4%–15% acrylamide) were purchased from Bio-Rad. Ni-NTA affinity resin was purchased from QIAGEN. HiTrap-Q anion-exchange column was purchased from Amersham Pharmacia.

Cloning, Expression, and Purification of the [KS3][AT3] Didomain of DEBS Module 3

The construction of an expression vector encoding the [KS3][AT3] didomain from DEBS module 3 (pAYC02) has been previously described [30]. The N-terminal KS linker was deleted from the [KS3][AT3] didomain, by using PCR to amplify pAYC02 from ELES to the natural AscI site, and an engineered NdeI site was introduced with primers 5′-GCAGCGCCATATGGAGCTGGAATCCGACCCGATCG-3′ and 5′-GCGGCGCGCCGAGTCCGCTCGCC-3′. The resulting NdeI-AscI fragment was cloned back into NdeI-AscI-digested pAYC02 to yield plasmid pAYC09, encoding the DEBS [KS3][AT3] didomain lacking the N-terminal docking domain. The sequence of pAYC09 was verified directly by DNA sequencing, and the plasmid was introduced into *E. coli* BL21(DE3) cells by electroporation. The resulting transformant was grown in LB medium at 37°C to an OD_{600} of 0.6. The culture was then cooled to 18°C, followed by induction with 0.2 mM isopropyl-β-D-thiogalactopyranoside, and was grown for an additional 14 hr at 18°C. The cells were harvested by centrifugation (4420 × g for 15 min), resuspended in lysis/wash buffer (50 mM phosphate [pH 7.6], 300 mM NaCl, 10 mM imidazole), and lysed by sonication (5 × 1 min). After the cell debris was removed, the supernatant was applied to a Nickel-NTA agarose (QIAGEN) column in batch mode. After extensive washing with 10 column volumes of lysis/wash buffer, the protein was eluted with 3 column volumes of elution buffer (50 mM phosphate [pH 7.6], 100 mM NaCl, 150 mM imidazole). After determination of the protein concentration by using a Biorad assay, a 100 molar excess of the inhibitor cerulenin was added, and the mixture was allowed to incubate overnight at 4°C to effect covalent modification. The resulting modified protein was further polished on a Hi-Trap-Q anion-exchange column (Amersham-Pharmacia) by using a linear gradient of NaCl, with elution of the protein-inhibitor complex at ~350 mM NaCl. The purified complex was exchanged into 20 mM HEPES buffer (pH 7.6) and was concentrated to 1 mg/ml. The typical yield of the KS-AT didomain-cerulenin complex was 20 mg/l culture.

Crystallization and Data Collection for the [KS3][AT3] Didomain of DEBS Module 3 Complexed with Cerulenin

Crystals were grown at room temperature by using the hanging-drop vapor-diffusion method with a ratio of 2 μl [KS3][AT3]-cerulenin complex solution (1 mg/ml) to 2 μl mother liquor. The well buffer contained 0.1 M HEPES (pH 7.0), 0.2 M Li_2SO_4, and 25% PEG 3350. The crystals belong to space group $P2_1$ and contain two monomers per symmetric unit. The unit cell has dimensions of a = 75.203 Å, b = 139.005 Å, c = 102.342 Å, β = 106.14°. For cryocooling, the crystals were harvested in a well solution with 10% glycerol. Diffraction data sets were collected on beamline 11-1 at the Stanford Synchrotron Radiation Laboratory (SSRL) to 2.6 Å and were processed with the HKL2000 package [52]. The crystallographic data are summarized in Table 1.

The [KS3][AT3] protein acylated with (2*S*,3*R*)-2-methyl-3-hydroxypentanoyl-*N*-acetylcysteamine thioester was also used in crystallization, but no diffractable crystals were obtained.

Structure Refinement and Model Building

Initial phases were obtained by molecular replacement by using the program Molrep in CCP4i [53] and the coordinates of the DEBS module 5 [KS5][AT5] didomain (PDB ID: 2HG4) as the search model. The sequence was replaced by that of the [KS3][AT3] didomain from DEBS module 3, and the structure was further refined by using CCP4i and was then fit manually with O [54] and Coot [55]. Noncrystallographic symmetry restraints were applied for the initial rounds of refinement and were removed for final stages. Both the $2F_o - F_c$ and $F_o - F_c$ maps showed the presence of a portion of the bound cerulenin in the active site of the KS3 domain. The three-dimensional structure of the relevant portions of the cerulenin adduct was then fit by hand into the visible electron density. Both sites in the asymmetric unit

showed a good fit between the map and the hand-fit cerulenin molecules. Water molecules were added by using Coot, followed by visual inspection with O at the final stage. A total of 5% of the reflections were excluded from refinement and constituted the R_{free} set. The final geometry was assessed with PROCHECK [56].

Molecular Docking Simulations

The homology model of the DEBS ACP3 domain was generated by using the WHATIF homology model server [57] based on the solution NMR structure of the DEBS ACP2 domain (PDB ID: 2JU2) [38]. The calculated docking between ACP3 and the [KS3][AT3] didomain was carried out by using both the 3D-Dock program suite [40] and the Patchdock server [41, 42] (http://bioinfo3d.cs.tau.ac.il/PatchDock/index.html). When the 3D-Dock program suite was used, the coordinates of the dimeric [KS3][AT3] didomain were defined as the static model, with ACP3 defined as the mobile model. The binding interface was exhaustively searched by using default parameters. The resulting complexes were then scored by an empirical pair potential matrix [58], and the best-scored complex was energy minimized by CCP4i [53]. When the Patchdock server was used, the dimeric [KS3][AT3] didomain was defined as the receptor and the ACP3 protein was defined as the ligand. The best-docking models returned by both programs were very similar, and each identified the deep cleft between the KS domain and the AT domain as the ACP3 docking site. The specific model that is discussed in detail in the text was calculated by using the Patchdock server. The docking between ACP2 and the [KS3][AT3] didomain was carried out in a similar manner.

Construction, Expression, and Purification of ACP3 Mutants F78D, R44D, R45Q, R44D/R45Q

Mutagenesis was performed with the QuikChange Site-Directed Mutagenesis Kit (Stratagene). Primers 5′-TCGCTGGTGGACGACCACCCCACCG-3′, 5′-CGCCGAGATCAACGTGGACCGCGCGTTCAGCG-3′, 5′-CGAGATCAACGTGCGCCAGGCGTTCAGCGAGCTCG-3′, and 5′-CGCCGAGATCAACGTGGACCAGGCGTTCAGCGAGCTCG-3′ and their complementary oligonucleotides were used to introduce the F78D, R44D, R45Q, and R44D/R45Q mutation(s), respectively, into DEBS ACP3. The expression and purification of the mutants were carried as described for wild-type ACP3 [13, 30].

Triketide Ketolactone Formation

[KS3][AT3] idomain (2 μM for the F78D mutant time course and 10 μM for experiments with the R44D, R45Q, and R44D/R45Q mutants, in 100 mM phosphate [pH 7.2]) was incubated with 5 mM (2*S*,3*R*)-2-methyl-3-hydroxypentanoyl-*N*-acetylcysteamine thioester and 5 mM TCEP for 1 hr at room temperature to acylate KS3 to completion. *Holo* ACP (four ACP concentrations ranging from 2 to 200 μM) and 200 μM DL-[2-methyl-^{14}C]methylmalonyl-CoA were then added and allowed to react at room temperature. At various time points, 10 μl reaction solution was drawn from the reaction mixture and quenched by adding 20 μl 0.5 M potassium hydroxide. The mixture was further processed as described previously [30].

Circular Dichroism Spectroscopy

The proteins were diluted in 20 mM potassium phosphate (pH 7.2). All of the proteins had a concentration of 0.25 mg/ml; circular dichroism ellipticity was recorded with an Aviv 202-01 instrument (Aviv Associates, Lakewood, NJ). Spectra from 270 to 190 nm were scanned at a step of 1 nm at 25°C in a 0.1 cm cuvette, with three repeats and an averaging time of 1 s.

Supplemental Data

Supplemental Data include Figures S1–S4 and Tables S1 and S2 and are available at http://www.chembiol.com/cgi/content/full/14/8/931/DC1/.

ACKNOWLEDGMENTS

We thank Dr. Irimpan I. Mathews for help with data collection and structure determination, Dr. Pavel Strop for helping with circular dichroism experiments, and Dr. Nathan A. Schnarr for helpful discussion and proofreading. This work was supported by grants from the National Institutes of Health: CA 66736 (to C.K.) and GM 22172 (to D.E.C.). Portions of this research were carried out at the Stanford Synchrotron Radiation Laboratory, a national user facility operated by Stanford University on behalf of the U.S. Department of Energy, Office of Basic Energy Sciences.

Received: January 16, 2007
Revised: July 10, 2007
Accepted: July 13, 2007
Published: August 24, 2007

REFERENCES

1. O'Hagan, D. (1991). The Polyketide Metabolites (New York: Ellis Horwood).
2. Cane, D.E. (1997). Introduction: polyketide and nonribosomal polypeptide biosynthesis. From collie to coli. Chem. Rev. *97*, 2463–2464.
3. Carreras, C.W., and Khosla, C. (1998). Purification and in vitro reconstitution of the essential protein components of an aromatic polyketide synthase. Biochemistry *37*, 2084–2088.
4. Gokhale, R.S., Tsuji, S.Y., Cane, D.E., and Khosla, C. (1999). Dissecting and exploiting intermodular communication in polyketide synthases. Science *284*, 482–485.
5. Hans, M., Hornung, A., Dziarnowski, A., Cane, D.E., and Khosla, C. (2003). Mechanistic analysis of acyl transferase domain exchange in polyketide synthase modules. J. Am. Chem. Soc. *125*, 5366–5374.
6. Ranganathan, A., Timoney, M., Bycroft, M., Cortes, J., Thomas, I.P., Wilkinson, B., Kellenberger, L., Hanefeld, U., Galloway, I.S., Staunton, J., and Leadlay, P.F. (1999). Knowledge-based design of bimodular and trimodular polyketide synthases based on domain and module swaps: a route to simple statin analogues. Chem. Biol. *6*, 731–741.
7. Kumar, P., Khosla, C., and Tang, Y. (2004). Manipulation and analysis of polyketide synthases. Methods Enzymol. *388*, 269–293.
8. Cortes, J., Haydock, S.F., Roberts, G.A., Bevitt, D.J., and Leadlay, P.F. (1990). An unusually large multifunctional polypeptide in the erythromycin-producing polyketide synthase of *Saccharopolyspora erythraea*. Nature *348*, 176–178.
9. Donadio, S., Staver, M.J., McAlpine, J.B., Swanson, S.J., and Katz, L. (1991). Modular organization of genes required for complex polyketide biosynthesis. Science *252*, 675–679.
10. McDaniel, R., Kao, C.M., Hwang, S.J., and Khosla, C. (1997). Engineered intermodular and intramodular polyketide synthase fusions. Chem. Biol. *4*, 667–674.
11. Ruan, X., Pereda, A., Stassi, D.L., Zeidner, D., Summers, R.G., Jackson, M., Shivakumar, A., Kakavas, S., Staver, M.J., Donadio, S., and Katz, L. (1997). Acyltransferase domain substitutions in erythromycin polyketide synthase yield novel erythromycin derivatives. J. Bacteriol. *179*, 6416–6425.
12. Tang, Y., Kim, C.Y., Mathews, I.I., Cane, D.E., and Khosla, C. (2006). The 2.7 Å crystal structure of a 194-kDa homodimeric fragment of the 6-deoxyerythronolide B synthase. Proc. Natl. Acad. Sci. USA *103*, 11124–11129.
13. Kim, C.Y., Alekseyev, V.Y., Chen, A.Y., Tang, Y., Cane, D.E., and Khosla, C. (2004). Reconstituting modular activity from separated domains of 6-deoxyerythronolide B synthase. Biochemistry *43*, 13892–13898.
14. Olsen, J.G., Kadziola, A., von Wettstein-Knowles, P., Siggaard-Andersen, M., Lindquist, Y., and Larsen, S. (1999). The X-ray crystal structure of β-ketoacyl [acyl carrier protein] synthase I. FEBS Lett. *460*, 46–52.

15. Huang, W., Jia, J., Edwards, P., Dehesh, K., Schneider, G., and Lindqvist, Y. (1998). Crystal structure of β-ketoacyl-acyl carrier protein synthase II from *E. coli* reveals the molecular architecture of condensing enzymes. EMBO J. *17*, 1183–1191.

16. Davies, C., Heath, R.J., White, S.W., and Rock, C.O. (2000). The 1.8 Å crystal structure and active-site architecture of β-ketoacyl-acyl carrier protein synthase III (FabH) from *Escherichia coli*. Structure *8*, 185–195.

17. Pan, H., Tsai, S., Meadows, E.S., Miercke, L.J., Keatinge-Clay, A.T., O'Connell, J., Khosla, C., and Stroud, R.M. (2002). Crystal structure of the priming β-ketosynthase from the R1128 polyketide biosynthetic pathway. Structure *10*, 1559–1568.

18. Keatinge-Clay, A.T., Maltby, D.A., Medzihradszky, K.F., Khosla, C., and Stroud, R.M. (2004). An antibiotic factory caught in action. Nat. Struct. Mol. Biol. *11*, 888–893.

19. Keatinge-Clay, A.T., Shelat, A.A., Savage, D.F., Tsai, S.C., Miercke, L.J., O'Connell, J.D., 3rd, Khosla, C., and Stroud, R.M. (2003). Catalysis, specificity, and ACP docking site of *Streptomyces coelicolor* malonyl-CoA:ACP transacylase. Structure *11*, 147–154.

20. Serre, L., Verbree, E.C., Dauter, Z., Stuitje, A.R., and Derewenda, Z.S. (1995). The *Escherichia coli* malonyl-CoA:acyl carrier protein transacylase at 1.5 Å resolution. Crystal structure of a fatty acid synthase component. J. Biol. Chem. *270*, 12961–12964.

21. Broadhurst, R.W., Nietlispach, D., Wheatcroft, M.P., Leadlay, P.F., and Weissman, K.J. (2003). The structure of docking domains in modular polyketide synthases. Chem. Biol. *10*, 723–731.

22. von Wettstein-Knowles, P., Olsen, J.G., McGuire, K.A., and Henriksen, A. (2006). Fatty acid synthesis. Role of active site histidines and lysine in Cys-His-His-type β-ketoacyl-acyl carrier protein synthases. FEBS J. *273*, 695–710.

23. Witkowski, A., Joshi, A.K., and Smith, S. (2002). Mechanism of the β-ketoacyl synthase reaction catalyzed by the animal fatty acid synthase. Biochemistry *41*, 10877–10887.

24. Price, A.C., Choi, K.H., Heath, R.J., Li, Z., White, S.W., and Rock, C.O. (2001). Inhibition of β-ketoacyl-acyl carrier protein synthases by thiolactomycin and cerulenin. Structure and mechanism. J. Biol. Chem. *276*, 6551–6559.

25. Moche, M., Schneider, G., Edwards, P., Dehesh, K., and Lindqvist, Y. (1999). Structure of the complex between the antibiotic cerulenin and its target, β-ketoacyl-acyl carrier protein synthase. J. Biol. Chem. *274*, 6031–6034.

26. Tsukamoto, N., Chuck, J.A., Luo, G., Kao, C.M., Khosla, C., and Cane, D.E. (1996). 6-deoxyerythronolide B synthase 1 is specifically acylated by a diketide intermediate at the β-ketoacyl-acyl carrier protein synthase domain of module 2. Biochemistry *35*, 15244–15248.

27. Hunziker, D., Wu, N., Kenoshita, K., Cane, D.E., and Khosla, C. (1999). Precursor directed biosynthesis of novel 6-deoxyerythronolide B analogs containing non-natural oxygen substituents and reactive functionalities. Tetrahedron Lett. *40*, 635–638.

28. Wu, N., Tsuji, S.Y., Cane, D.E., and Khosla, C. (2001). Assessing the balance between protein-protein interactions and enzyme-substrate interactions in the channeling of intermediates between polyketide synthase modules. J. Am. Chem. Soc. *123*, 6465–6474.

29. Wu, N., Cane, D.E., and Khosla, C. (2002). Quantitative analysis of the relative contributions of donor acyl carrier proteins, acceptor ketosynthases, and linker regions to intermodular transfer of intermediates in hybrid polyketide synthases. Biochemistry *41*, 5056–5066.

30. Chen, A.Y., Schnarr, N.A., Kim, C.Y., Cane, D.E., and Khosla, C. (2006). Extender unit and acyl carrier protein specificity of ketosynthase domains of the 6-deoxyerythronolide B synthase. J. Am. Chem. Soc. *128*, 3067–3074.

31. Li, Q., Khosla, C., Puglisi, J.D., and Liu, C.W. (2003). Solution structure and backbone dynamics of the holo form of the frenolicin acyl carrier protein. Biochemistry *42*, 4648–4657.

32. Xu, G.Y., Tam, A., Lin, L., Hixon, J., Fritz, C.C., and Powers, R. (2001). Solution structure of *B. subtilis* acyl carrier protein. Structure *9*, 277–287.

33. Holak, T.A., Kearsley, S.K., Kim, Y., and Prestegard, J.H. (1988). Three-dimensional structure of acyl carrier protein determined by NMR pseudoenergy and distance geometry calculations. Biochemistry *27*, 6135–6142.

34. Sharma, A.K., Sharma, S.K., Surolia, A., Surolia, N., and Sarma, S.P. (2006). Solution structures of conformationally equilibrium forms of holo-acyl carrier protein (PfACP) from *Plasmodium falciparum* provides insight into the mechanism of activation of ACPs. Biochemistry *45*, 6904–6916.

35. Crump, M.P., Crosby, J., Dempsey, C.E., Parkinson, J.A., Murray, M., Hopwood, D.A., and Simpson, T.J. (1997). Solution structure of the actinorhodin polyketide synthase acyl carrier protein from *Streptomyces coelicolor* A3(2). Biochemistry *36*, 6000–6008.

36. Findlow, S.C., Winsor, C., Simpson, T.J., Crosby, J., and Crump, M.P. (2003). Solution structure and dynamics of oxytetracycline polyketide synthase acyl carrier protein from *Streptomyces rimosus*. Biochemistry *42*, 8423–8433.

37. Wong, H.C., Liu, G., Zhang, Y.M., Rock, C.O., and Zheng, J. (2002). The solution structure of acyl carrier protein from *Mycobacterium tuberculosis*. J. Biol. Chem. *277*, 15874–15880.

38. Drake, E.J., Nicolai, D.A., and Gulick, A.M. (2006). Structure of the EntB multidomain nonribosomal peptide synthetase and functional analysis of its interaction with the EntE adenylation domain. Chem. Biol. *13*, 409–419.

39. Alekseyev, V.Y., Liu, C.W., Cane, D.E., Puglisi, J.D., and Khosla, C. (2007). Solution Structure and Proposed Domain-domain Recognition Interface of an Acyl Carrier Protein Domain from a Modular Polyketide Synthase. Protein Sci., in press.

40. Katchalski-Katzir, E., Shariv, I., Eisenstein, M., Friesem, A.A., Aflalo, C., and Vakser, I.A. (1992). Molecular surface recognition: determination of geometric fit between proteins and their ligands by correlation techniques. Proc. Natl. Acad. Sci. USA *89*, 2195–2199.

41. Duhovny, D., Nussinov, R., and Wolfson, H.J. (2002). Efficient unbound docking of rigid molecules. Lecture Notes Comput. Sci. *2452*, 185–200.

42. Schneidman-Duhovny, D., Inbar, Y., Polak, V., Shatsky, M., Halperin, I., Benyamini, H., Barzilai, A., Dror, O., Haspel, N., Nussinov, R., and Wolfson, H.J. (2003). Taking geometry to its edge: fast unbound rigid (and hinge-bent) docking. Proteins *52*, 107–112.

43. Leibundgut, M., Jenni, S., Frick, C., and Ban, N. (2007). Structural basis for substrate delivery by acyl carrier protein in the yeast fatty acid synthase. Science *316*, 288–290.

44. Kao, C.M., Pieper, R., Cane, D.E., and Khosla, C. (1996). Evidence for two catalytically independent clusters of active sites in a functional modular polyketide synthase. Biochemistry *35*, 12363–12368.

45. Khosla, C., Tang, Y., Chen, A.Y., Schnarr, N.A., and Cane, D.E. (2007). Structure and mechanism of the 6-deoxyerythronolide B synthase. Annu. Rev. Biochem. *76*, 195–221.

46. Chen, A.Y., Cane, D.E., and Khosla, C. (2007). Structure-based dissociation of a type I polyketide synthase module. Chem. Biol. *14*, 784–792.

47. Lai, J.R., Fischbach, M.A., Liu, D.R., and Walsh, C.T. (2006). A protein interaction surface in nonribosomal peptide synthesis mapped by combinatorial mutagenesis and selection. Proc. Natl. Acad. Sci. USA *103*, 5314–5319.

48. Zhou, Z., Lai, J.R., and Walsh, C.T. (2006). Interdomain communication between the thiolation and thioesterase domains of EntF explored by combinatorial mutagenesis and selection. Chem. Biol. *13*, 869–879.

49. Harris, R.C., Cutter, A.L., Weissman, K.J., Hanefeld, U., Timoney, M.C., and Staunton, J. (1998). Enantiospecific synthesis of analogs of the diketide intermediate of the erythromycin polyketide synthase (PKS). J. Chem. Res. *283*, 1230–1247.

50. Jacobsen, J.R., Hutchinson, C.R., Cane, D.E., and Khosla, C. (1997). Precursor-directed biosynthesis of erythromycin analogs by an engineered polyketide synthase. Science *277*, 367–369.

51. Cane, D.E., Kudo, F., Kinoshita, K., and Khosla, C. (2002). Precursor-directed biosynthesis: biochemical basis of the remarkable selectivity of the erythromycin polyketide synthase toward unsaturated triketides. Chem. Biol. *9*, 131–142.

52. Otwinowski, Z., and Minor, W. (1997). Processing of X-ray diffraction data collected in oscillation mode. Methods Enzymol. *276*, 307–326.

53. CCP4 (Collaborative Computational Project, Number 4) (1994). The CCP4 suite: programs for protein crystallography. Acta Crystallogr. D Biol. Crystallogr. *50*, 760–763.

54. Jones, T.A., Zou, J.Y., Cowan, S.W., and Kjeldgaard, M. (1991). Improved methods for building protein models in electron density maps and the location of errors in these models. Acta Crystallogr. A *47*, 110–119.

55. Emsley, P., and Cowtan, K. (2004). Coot: model-building tools for molecular graphics. Acta Crystallogr. D Biol. Crystallogr. *60*, 2126–2132.

56. Laskowski, R., MacArthur, M., Moss, D., and Thornton, J. (1993). PROCHECK: a program to check the stereochemical quality of protein structures. J. Appl. Cryst. *26*, 283–291.

57. Rodriguez, R., Chinea, G., Lopez, N., Pons, T., and Vriend, G. (1998). Homology modeling, model and software evaluation: three related resources. Bioinformatics *14*, 523–528.

58. Moont, G., Gabb, H.A., and Sternberg, M.J. (1999). Use of pair potentials across protein interfaces in screening predicted docked complexes. Proteins *35*, 364–373.

Accession Numbers

Atomic coordinates of the [KS3][AT3] didomain from DEBS module 3 have been deposited in the Protein Data Bank under accession code 2QO3.